

Can We Improve the Preprocessing of Photospheric Vector Magnetograms by the Inclusion of Chromospheric Observations?

T. Wiegelmann¹ · J.K. Thalmann¹ ·
C.J. Schrijver² · M.L. DeRosa² · T.R. Metcalf³
†

DOI: 10.1007/s11207-008-9130-y
Bibliographic Code: 2008SoPh..247..249W

© Springer ●●●●

Abstract The solar magnetic field is key to understanding the physical processes in the solar atmosphere. Nonlinear force-free codes have been shown to be useful in extrapolating the coronal field upward from underlying vector boundary data. However, we can only measure the magnetic field vector routinely with high accuracy in the photosphere, and unfortunately these data do not fulfill the force-free condition. We must therefore apply some transformations to these data before nonlinear force-free extrapolation codes can be self-consistently applied. To this end, we have developed a minimization procedure that yields a more chromosphere-like field, using the measured photospheric field vectors as input. The procedure includes force-free consistency integrals, spatial smoothing, and — newly included in the version presented here — an improved match to the field direction as inferred from fibrils as can be observed in, *e.g.*, chromospheric H α images. We test the procedure using a model active-region field that included buoyancy forces at the photospheric level. The proposed preprocessing method allows us to approximate the chromospheric vector field to within a few degrees and the free energy in the coronal field to within one percent.

Keywords: Magnetic fields, Photosphere, Chromosphere, Corona

1. Introduction

The solar interior, photosphere and atmosphere are coupled by magnetic fields. It is therefore important to gain insights about the magnetic field structure in all layers of the Sun and solar atmosphere. Direct and accurate measurements of the magnetic field vector are typically carried out only on the photosphere. Although measurements in higher layers are available for a few individual cases, *e.g.* in the chromosphere by Solanki *et al.* (2003) and in the corona by Lin, Kuhn, and Coulter (2004), the line-of-sight integrated character of such chromospheric and coronal magnetic field measurements complicates their interpretation (Kramar, Inhester, and Solanki, 2006). Knowledge of the magnetic field in the corona is essential, however, to

†Unfortunately our colleague, co-author, and friend Tom Metcalf deceased before the final manuscript was finished. We continued our joint work in his memory and would like to remember him here.

¹ Max-Planck-Institut für Sonnensystemforschung,
Max-Planck-Strasse 2, 37191 Katlenburg-Lindau, Germany
email: wiegelmann@mps.mpg.de email: thalmann@mps.mpg.de

² Lockheed Martin Advanced Technology Center, Dept.
ADBS, Bldg. 252, 3251 Hanover St., Palo Alto, CA 94304,
USA email: schryver@lmsal.com email: derosa@lmsal.com

³ Northwest Research Associates, Colorado Research
Associates Division, 3380 Mitchell Ln., Boulder, CO 90301
USA

understand basic physical processes such as the onset of flares, coronal mass ejections and eruptive prominences.

Inferences of the coronal magnetic field can be obtained by extrapolating measurements of the photospheric magnetic field vector (*e.g.* observed by *Hinode*/SOT, SOLIS or the upcoming SDO/HMI instruments) into the corona. Because the magnetic pressure dominates the plasma pressure in active-region coronae, making the plasma β low, [See work by Gary (2001) and Schrijver and van Ballegooijen (2005), which discuss the plasma beta over active regions and over the quiet Sun, respectively], these extrapolations neglect non-magnetic forces and assume the coronal magnetic field \mathbf{B} to be force-free, such that it obeys:

$$\nabla \cdot \mathbf{B} = 0, \quad (1)$$

$$(\nabla \times \mathbf{B}) \times \mathbf{B} = 0. \quad (2)$$

Equation (2) implies that the electric current density $\mu_0 \mathbf{j} = \nabla \times \mathbf{B}$ is parallel to the magnetic field \mathbf{B} . Starting more than a quarter century ago (Sakurai, 1981), different mathematical methods and numerical implementations have been developed to solve the nonlinear force-free equations (1) and (2) for the solar case. See, for example, (Sakurai, 1989; Amari *et al.*, 1997; Wiegelmann, 2008) for review papers and (Schrijver *et al.*, 2006; Metcalf *et al.*, 2007) for evaluations of the performance of corresponding computer programs with model data. The codes use the magnetic field vector (or quantities derived from the magnetic field vector) on the bottom boundary of a computational domain as input. One would like to prescribe the measured photospheric data as the bottom boundary of nonlinear force-free fields (NLFFF) codes, but there is a problem: the observed photospheric magnetic field is usually not force-free. The relatively high plasma β in the photosphere means that non-magnetic forces cannot be neglected there and that such photospheric magnetic field data are not consistent with well known force-free compatibility conditions defined in (Aly, 1989). Recently, Wiegelmann, Inhester, and Sakurai (2006) developed a scheme that mitigates this problem, in which the inconsistent and noisy photospheric vector magnetograms used as bottom boundary conditions are preprocessed in order to remove net magnetic forces and torques and to smooth out small-scale noise-like magnetic structures. The resulting magnetic field data are sufficiently force-free and smooth for use with extrapolation codes, but also are found to bear a high resemblance to chromospheric vector magnetic field data. This leads us to the question whether we can constrain the preprocessing tool further by taking direct chromospheric observations, such as H α images, into consideration. We will investigate this topic in the present work.

2. A Short Review About Consistency Criteria for Force-free Coronal Extrapolations

In this section, we briefly discuss the criteria on the photospheric boundary data that are required for consistency with a force-free extrapolation of the overlying coronal magnetic field. Molodensky (1969), Molodensky (1974), Aly (1989), and Sakurai (1989) show how moments of the Lorentz force, integrated over a volume of interest, define constraints on the closed surface bounding this volume. As explained in detail

in Molodensky (1974) the sense of these relations is that on average a force-free field cannot exert pressure on the boundary or shear stresses along axes lying in the boundary. For the coronal magnetic field extrapolation calculations discussed here, a localized region of interest, such as an active region, is typically selected for analysis. The extrapolation algorithms applied to the coronal volume overlying such localized regions of interest require boundary conditions, and, except at the lower (photospheric) boundary, these boundary conditions are usually chosen to be consistent with potential fields and thus do not possess magnetic forces or torques. In these cases, the consistency criteria reduce to conditions on the lower boundary only:

1. On average force-free fields cannot exert pressure on the boundary

$$F_1 = \int_S B_x B_z \, dx \, dy = 0, \quad (3)$$

$$F_2 = \int_S B_y B_z \, dx \, dy = 0 \quad (4)$$

$$F_3 = \int_S (B_x^2 + B_y^2) \, dx \, dy - \int_S B_z^2 \, dx \, dy = 0. \quad (5)$$

2. On average force-free fields cannot create shear stresses along axes lying in the boundary

$$T_1 = \int_S x (B_x^2 + B_y^2) \, dx \, dy - \int_S x B_z^2 \, dx \, dy = 0, \quad (6)$$

$$T_2 = \int_S y (B_x^2 + B_y^2) \, dx \, dy - \int_S y B_z^2 \, dx \, dy = 0, \quad (7)$$

$$T_3 = \int_S y B_x B_z \, dx \, dy - \int_S x B_y B_z \, dx \, dy = 0. \quad (8)$$

These relations must be fulfilled in order to be suitable boundary conditions for a nonlinear force-free coronal magnetic field extrapolation. We define dimensionless numbers,

$$\epsilon_{\text{force}} = \frac{|F_1| + |F_2| + |F_3|}{\int_S (B_x^2 + B_y^2 + B_z^2) \, dx \, dy}, \quad (9)$$

$$\epsilon_{\text{torque}} = \frac{|T_1| + |T_2| + |T_3|}{\int_S \sqrt{x^2 + y^2} (B_x^2 + B_y^2 + B_z^2) \, dx \, dy}. \quad (10)$$

in order to evaluate how well these criteria are met. Ideally, it is necessary for $\epsilon_{\text{force}} = \epsilon_{\text{torque}} = 0$ for a force-free coronal magnetic field to exist.

Aly (1989) pointed out that the magnetic field is probably not force-free in the photosphere, where \mathbf{B} is measured because the plasma β in the photosphere is of the order of unity and pressure gradient and gravity forces are not negligible. The integral relations (3)-(8) are not satisfied in this case in the photosphere and the

measured photospheric field is not a suitable boundary condition for a force-free extrapolation. Investigations by Metcalf *et al.* (1995) revealed that the solar magnetic field is not force-free in the photosphere, but becomes force-free about 400km above the photosphere. The problem has been addressed also by Gary (2001) who pointed out that care has to be taken when extrapolating the coronal magnetic field as a force-free field from photospheric measurements, because the force-free low corona is sandwiched between two regions (photosphere and higher corona) with a plasma $\beta \approx 1$, where the force-free assumption might break down. An additional problem is that measurements of the photospheric magnetic vector field contain inconsistencies and noise. In particular the components of \mathbf{B} transverse to the line of sight, as measured by current vector magnetographs, are more uncertain than the line-of-sight component. As measurements in higher layers of the solar atmosphere (where the magnetic field is force-free) are not routinely available, we have to deal with the problem of inconsistent (with the force-free assumption as defined by Equations (3)–(8)) photospheric measurements. A routine which uses measured photospheric vector magnetograms to find suitable boundary conditions for a nonlinear force-free coronal magnetic field extrapolation, dubbed “preprocessing”, has been developed by Wiegelmann, Inhester, and Sakurai (2006).

3. Preprocessing

3.1. Classical Preprocessing

The preprocessing scheme of Wiegelmann, Inhester, and Sakurai (2006) involves minimizing a two-dimensional functional of quadratic form similar to the following:

$$L_{\text{prep}} = \mu_1 L_1 + \mu_2 L_2 + \mu_3 L_3 + \mu_4 L_4 + \mu_5 L_5, \quad (11)$$

where

$$L_1 = \left[\left(\sum_p B_x B_z \right)^2 + \left(\sum_p B_y B_z \right)^2 + \left(\sum_p B_z^2 - B_x^2 - B_y^2 \right)^2 \right], \quad (12)$$

$$L_2 = \left[\left(\sum_p x (B_z^2 - B_x^2 - B_y^2) \right)^2 + \left(\sum_p y (B_z^2 - B_x^2 - B_y^2) \right)^2 + \left(\sum_p y B_x B_z - x B_y B_z \right)^2 \right], \quad (13)$$

$$L_3 = \left[\sum_p (B_x - B_{x\text{obs}})^2 + \sum_p (B_y - B_{y\text{obs}})^2 + \sum_p (B_z - B_{z\text{obs}})^2 \right], \quad (14)$$

$$L_4 = \left[\sum_p (\Delta B_x)^2 + (\Delta B_y)^2 + (\Delta B_z)^2 \right]. \quad (15)$$

The surface integrals as defined in Equations (3)–(8) are here replaced by a summation \sum_p over all grid nodes p of the bottom surface grid. We normalize the magnetic field strength with the average magnetic field on the photosphere and the length scale with the size of the magnetogram. Each constraint L_n is weighted by a yet undetermined factor μ_n . The first term ($n=1$) corresponds to the force-balance conditions (3)–(5), the next ($n=2$) to the torque-free condition (6)–(8). The following term ($n=3$) contains the difference of the optimized boundary condition with the measured photospheric data and the next term ($n=4$) controls the smoothing. The 2D-Laplace operator is designated by Δ and the differentiation in the smoothing term is achieved by the usual 5-point stencil. The last term ($n=5$) has not been used in preprocessing so far and will be introduced in the next section. The aim of the preprocessing procedure is to minimize L_{prep} so that all terms L_n if possible are made small simultaneously. This minimization procedure provides us iterative equations for B_x, B_y, B_z (see Wiegmann, Inhester, and Sakurai (2006) for details). As result of the preprocessing we get a data set which is consistent with the assumption of a force-free magnetic field in the corona but also as close as possible to the measured data within the noise level.

Nonlinear force-free extrapolation codes can be applied only to low plasma β regions, where the force-free assumption is justified. This is known not to be the case in the photosphere, but is mostly true for the upper chromosphere and for the corona in quiescent conditions. The preprocessing scheme as used until now modifies observed photospheric vector magnetograms with the aim of approximating the magnetic field vector at the bottom of the force-free domain, *i.e.*, at a height that we assume to be located in the middle to upper chromosphere. In this study, we investigate whether the use of chromospheric fibril observations as an additional constraint in the preprocessing can bring the resulting field into even better agreement with the expected chromospheric vector field.

We discuss this idea in the next section.

3.2. H α -Preprocessing

The idea is to specify another term ($\mu_5 L_5$) in Equation (11) which measures how well the preprocessed magnetic field is aligned with fibrils seen in H α . As a first step we have to extract the directions of the fibrils, say H_x and H_y out of the H α images, where \mathbf{H} is a unit vector tangent ($|\mathbf{H}| = 1$) to the chromospheric fibrils projected onto the solar photosphere (representing the field direction with a 180-degree ambiguity). For simplicity one might rebin H_x and H_y to the same resolution as the vector magnetogram. In regions where we cannot identify clear filamentary structures in the images we set $H_x = H_y = 0$. These regions are only affected by the other, classical terms of the preprocessing functional (11). The angle of the projected magnetic field vector on the xy-plane with the H α image is

$$\sin(\phi) = \frac{|\mathbf{B}_{\parallel} \times \mathbf{H}|}{|\mathbf{B}_{\parallel}| |\mathbf{H}|} \quad (16)$$

where $\mathbf{B}_{\parallel} = (B_x, B_y)$ is the projection of the magnetic field vector in the xy-plane and $\mathbf{H} = (H_x, H_y)$ are the directions of the chromospheric H α fibrils. The preprocessing aims for deriving the magnetic field vector on the bottom boundary of the force-free domain, which is located in the chromosphere. The chromospheric magnetic field is certainly a priori unknown and as initial condition for the preprocessing routine we take \mathbf{B}_{\parallel} from the photospheric vector magnetogram.

We define the functional:

$$L_5 = \sum_p w(B_x H_y - B_y H_x)^2 = \sum_p w \mathbf{B}_{\parallel}^2 \sin^2(\phi). \quad (17)$$

Please note that the term $B_x H_y - B_y H_x$ in Equation (17) weights the angle with the magnetic field strength, because it is in particular important to minimize the angle in strong field regions. The space dependent function $w = w(x, y)$ is not a priori related to the magnetic field strength. w can be specified in order to indicate the confidence level of the fibril direction-finding algorithm (see *e.g.*, Inhester, Feng, and Wiegelmann (2007) for the description of a corresponding feature recognition tool). For the application to observational data w will be (with appropriate normalization) provided by this tool. It is likely, however, that the direction of the H α fibrils can be identified more accurately in strong magnetic field regions, but this is not an a priori assumption. In Section 4.3 we investigate the influence of different assumptions for w .

We take the functional derivative of L_5

$$\frac{dL_5}{dt} = 2(B_x H_y - B_y H_x) \left(H_y \frac{dB_x}{dt} - H_x \frac{dB_y}{dt} \right). \quad (18)$$

For a sufficiently small time step dt we get a decreasing L_5 with the iteration equations

$$\frac{dB_x}{dt} = -2w \mu_5 (B_x H_y - B_y H_x) H_y, \quad (19)$$

$$\frac{dB_y}{dt} = 2w \mu_5 (B_x H_y - B_y H_x) H_x. \quad (20)$$

The aim of our procedure is to make all terms in functional (11) small simultaneously. There are obvious contradictions between some of the L_n terms, such as between the $n = 3$ (photospheric data) and $n = 4$ (smoothing) terms. An important task is to find suitable values for the five parameters μ_n which control the relative weighting of the terms in Equation (11). The absolute values do not matter; only the relative weightings are important. We typically give all integral relations of the force and torque conditions (3)-(8) the same weighting (unity). To fulfill these consistency integrals is essential in order to find suitable boundary conditions for a nonlinear force-free extrapolation. In principle it would be possible to examine different values for the force-free term μ_1 and torque-free term μ_2 -or even to give six different weightings for the six integral relations- but giving all integrals the same weighting seems to be a reasonable choice. The torque integrals depend on the choice of the length scale D and giving the same weighting to all integrals requires $\mu_2 = \frac{\mu_1}{D^2}$. For the length scale normalization used here ($D = 1$) this leads to $\mu_1 = \mu_2$.

197 We will test our newly developed method with the help of a model active region
198 in the next section.

199 4. Tests

200 4.1. An Active Region Model for Testing the New Method

201 We test our extended preprocessing routine with the help of an active region model
202 recently developed by van Ballegoijen *et al.* (2007). In this model line-of-sight pho-
203 tospheric measurements from SOHO/MDI have been used to compute a potential
204 field. A twisted flux rope was then inserted into the volume, after which the whole
205 system was relaxed towards a nonlinear force-free state with the magnetofrictional
206 method described in van Ballegoijen (2004). The van Ballegoijen *et al.* (2007)
207 model is force-free throughout the entire computational domain, except within two
208 gridpoints of the bottom boundary. Hereafter, we refer to the bottom of the force-free
209 layer as the “model chromosphere” (see the top panel of Figure 1). On the bottom
210 boundary (see the central panel of Figure 1), hereafter referred to as the “model
211 photosphere”, the model contains significant non-magnetic forces and the force-free
212 consistency criteria (3)-(8) are not satisfied. These forces take the form of vertical
213 buoyancy forces directed upward, and have been introduced by van Ballegoijen *et al.*
214 *et al.* (2007) to mimic the effect of a reduced gas pressure in photospheric flux tubes.
215 The nature of these forces is therefore expected to be similar to those observed on the
216 real Sun. For a more detailed discussion we refer to Metcalf *et al.* (2007). Both the
217 chromospheric (\mathbf{B}_{ch}) as well as the photospheric magnetic field vector (\mathbf{B}_{ph}) from
218 the van Ballegoijen *et al.* (2007) model have been used to test four sophisticated
219 nonlinear force-free extrapolation codes in a blind algorithm test by Metcalf *et al.*
220 (2007).¹ The codes computed nonlinear force-free codes in a $320 \times 320 \times 256$ box,
221 which is about at the upper limit current codes can handle on workstations. We
222 briefly summarize the results of Metcalf *et al.* (2007) as:

- 223 • NLFFF-extrapolations from model-chromospheric data recover the original ref-
224 erence field with high accuracy.
- 225 • When the extrapolations are applied to the model-photospheric data, the ref-
226 erence field is not well recovered.
- 227 • Preprocessing of the model-photospheric data to remove net forces and torques
228 improves the result, but the resulting accuracy was lower than for extrapolations
229 from the model-chromospheric data.

230 The poor performance of extrapolations using the unprocessed model-photospheric
231 data is related to their inconsistency with respect to the force-free conditions (3)-
232 (8). The central panel of Figure 1 shows the photospheric magnetic field and the
233 central panel of Figure 2 illustrates the difference between the model-chromospheric
234 and model-photospheric fields. It is evident that there are remarkable differences
235 in all components of the magnetic field vector. For real data we usually cannot
236 measure the chromospheric magnetic field vector directly (which was possible for

¹Previously, the NLFFF codes have been intensively tested and evaluated with the (Low and Lou, 1990) semi-analytic equilibria (Schrijver *et al.*, 2006).

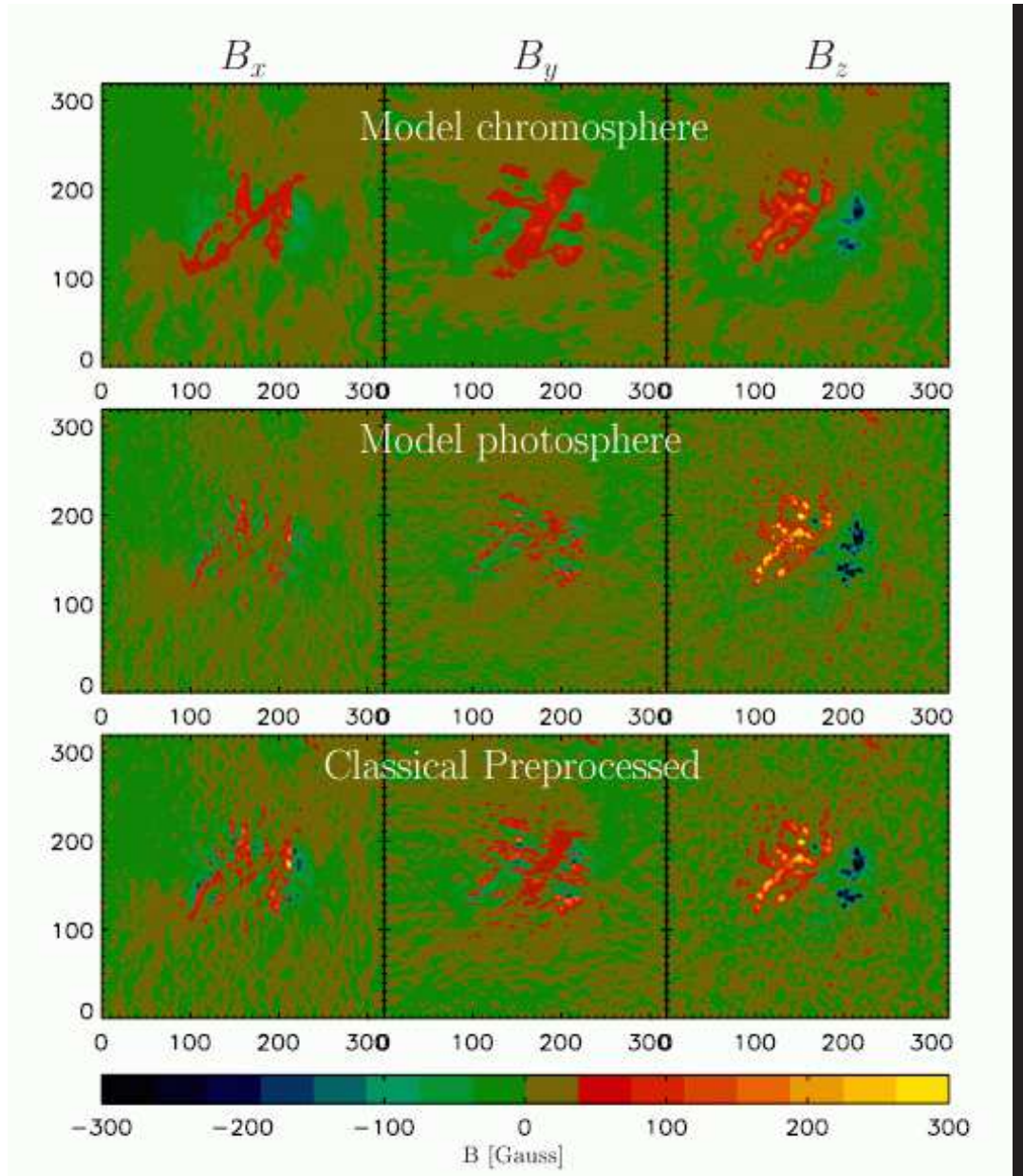


Figure 1. Top: Model-chromospheric magnetic field located in the $z = 2$ layer, Center: Model-photospheric magnetic field, Bottom: Model-photospheric magnetic field after classical preprocessing with $\mu_3 = 0.025$, $\mu_4 = 0.155$.

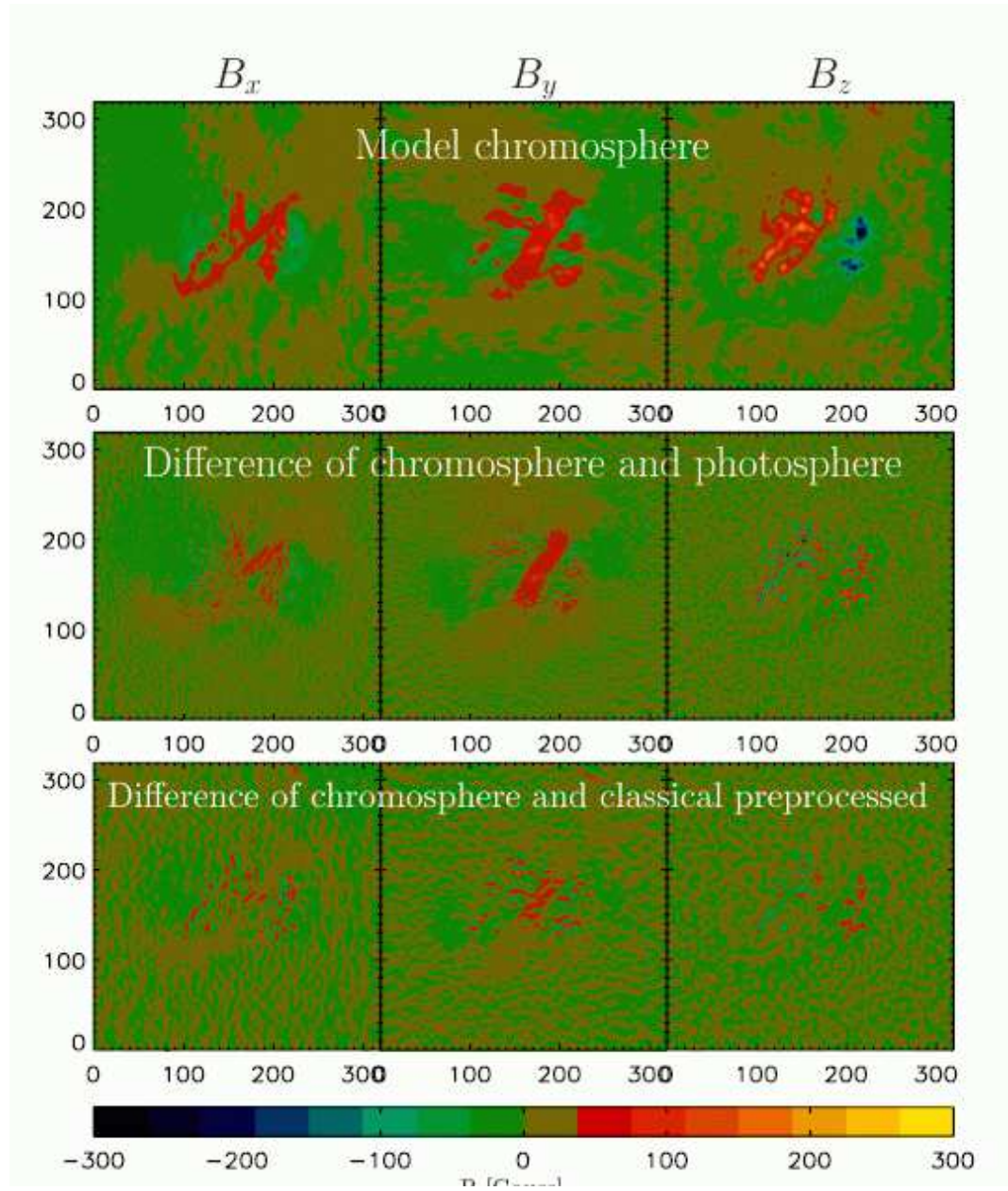


Figure 2. Top: Model-chromospheric magnetic field, Center: Difference between the chromospheric and photospheric model vector field, Bottom: Difference between the chromospheric and classical preprocessed photospheric field.

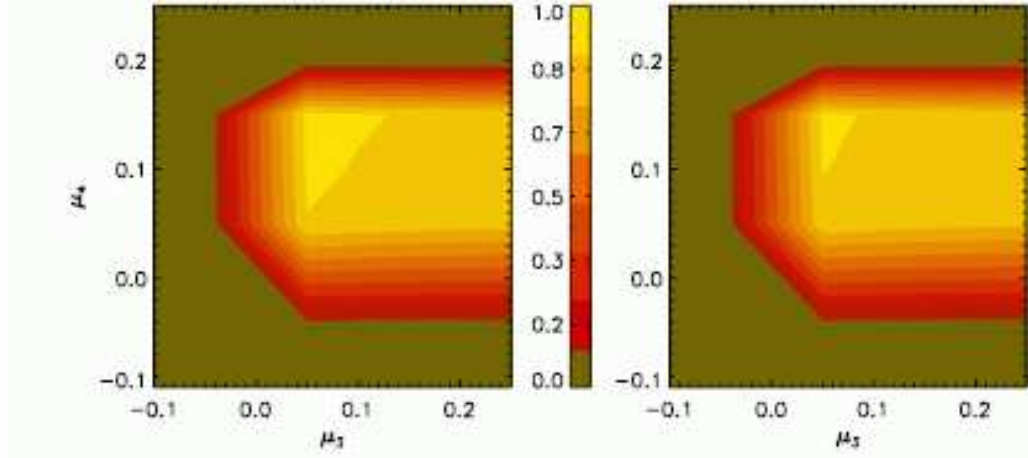


Figure 3. Correlation of the preprocessed field (left panel: B_x , right panel: B_y) with the model chromosphere in dependence of the preprocessing parameters μ_3 and μ_4 . We found a maximum correlation at $\mu_3 = 0.025$ and $\mu_4 = 0.155$.

(van Ballegoijen *et al.*, 2007) model data) and we have to apply preprocessing before using the data as input for force-free extrapolation codes. Force-free extrapolations using preprocessed data from the model photosphere (as lower panels of Figures 1 and 2), while encouraging, were not completely satisfactory, in light of the results being worse than when the model-chromospheric data were used as boundary conditions. In what follows, we will use an artificial $H\alpha$ image created from the model chromosphere to test a modified preprocessing scheme, and compare the results to the classical (original) preprocessing scheme.

We use the model-chromospheric magnetic field (\mathbf{B}_{ch}) to derive the direction vectors of the artificial $H\alpha$ images. For the model case we can simply use the chromospheric model field to specify the direction vectors H_x and H_y , which contain only information regarding the direction of the horizontal components of the magnetic field (including a 180° ambiguity, but no information about the magnetic field strength. For real data this information can be derived from high-resolution $H\alpha$ images using feature recognition techniques, *e.g.* the ridge detector of Inhester, Feng, and Wiegelmann (2007).

4.2. Optimal Parameter Set for Classical Preprocessing

We tested more than 1000 possible combinations of μ_3 and μ_4 using the model-photospheric field as input, and computed the Pearson correlation coefficient between the preprocessed results and the model-chromospheric field. Only B_x and B_y were used in computing the correlation coefficient, because the correlation of the longitudinal (*i.e.*, the line-of-sight) component is in general higher than that of the transverse components, due to B_z not being affected by the ambiguity-problem and the noise being much lower than in the other directions.

We computed 100 combinations of μ_3 and μ_4 between $-0.2 \leq \mu_3, \mu_4 \leq 0.2$ with a step size of $\Delta\mu_3 = \Delta\mu_4 = 0.05$. Hereafter a local maximum around $\mu_3 = 0.05$ and $\mu_4 = 0.15$ appeared. This region was analyzed in more detail by using these

two values as new initial guess. To do this, we tried another 100 combinations around this pair with a reduced step size of $\Delta\mu_3 = \Delta\mu_4 = 0.005$ in the positive as well as the negative direction. Then the absolute maximum of the correlation coefficients for both, B_x and B_y appeared at $\mu_3 = 0.025$ and $\mu_4 = 0.155$ (see Figure 3). The bottom panel of Figure 1 shows the corresponding preprocessed photospheric magnetic field.

4.3. Optimal Parameters and Weighting Functions for H α Preprocessing.

In the following we aim to find suitable parameters for including information from H α images into the preprocessing.

Our main aim is to investigate the effects of additional chromospheric information. To exclude side effects we therefore keep the combination of μ_1 - μ_4 found in the previous section to be able to clearly investigate the effect of the additional term L_5 . In principle one could vary all μ_n simultaneously. We cannot exclude that there might exist a better combination of μ_1 to μ_5 with better agreement of our preprocessed field and the model chromospheric field. This is, however, not the aim of this work, because this is not a suitable way to deal with real data, because there is no model chromosphere to test the result. It is not possible to provide an optimal parameter set suitable for all vector magnetographs. The optimal combination has to be carried out for different instruments separately. We expect that an optimal parameter set for a certain instrument and particular region will be also useful for the preprocessing of other regions of the same kind (say active regions) observed with the same instrument.

We test our methods with “model fibrils” extracted from the model chromosphere shown in the top panel of Figure 4. We define $w(x, y)$ used in Equation (17) as one of the following:

1. We assume that at every point of our H α image gives us the exact orientation of the magnetic field (which is indeed the case, as we calculated it from the chromospheric model data) and fix our weighting with $w(x, y) = w_1 = 1$.
2. We assume that the photospheric magnetic field magnitude gives us the importance of the H α information at each point and use

$$w(x, y) = w_2 = \sqrt{(B_x^2 + B_y^2 + B_z^2)_{\text{ph}}}.$$

We scale w_2 to a maximum value of 1. (See Figure 4 bottom left panel.)

3. We do as in the previous case, but assume now, that only points in the magnetogram where the field magnitude is greater than 50 % of the maximum contribute to the H α preprocessing. So, we define

$$w(x, y) = w_3 = \begin{cases} 1 & \text{for } w_2 \geq 0.5 \\ 0 & \text{for } w_2 < 0.5 \end{cases}.$$

(See Figure 4 bottom center panel.)

4. In our last case we assume in the same way as in the previous one, but now only points in the magnetogram where the field magnitude is greater than 10 % of the maximum contribute to the preprocessing. All these grid points are weighted with 1 and the rest with zero. In other words, one defines

$$w(x, y) = w_4 = \begin{cases} 1 & \text{for } w_2 \geq 0.1 \\ 0 & \text{for } w_2 < 0.1 \end{cases}.$$

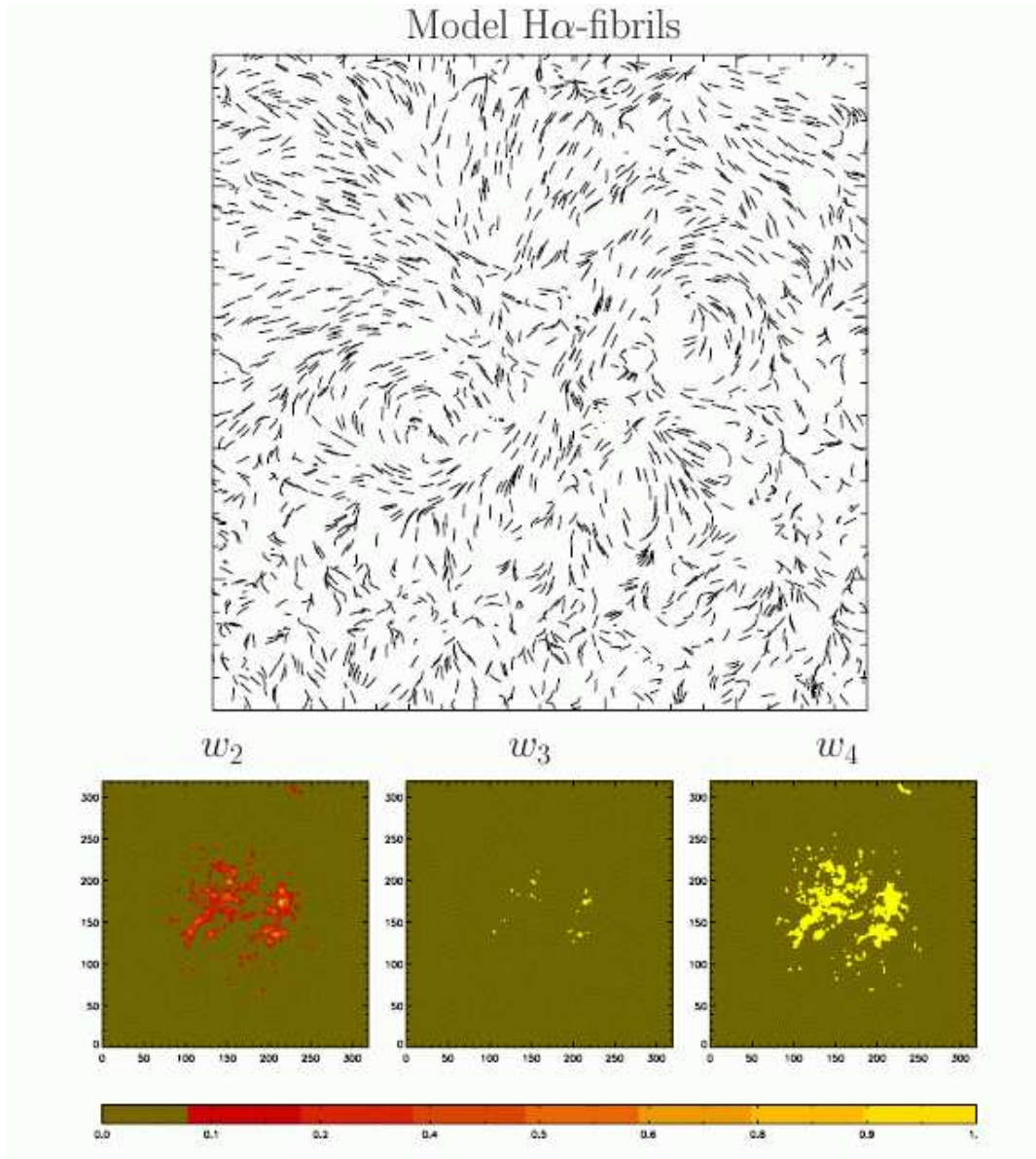


Figure 4. Top: H α fibrils identified from the model chromosphere. The fibrils give us information about the transverse components (B_x and B_y) of the chromospheric magnetic field. The fibrils contain a 180° ambiguity and do not provide any information about the chromospheric magnetic field strength. The bottom panels show from left to right the different weighting functions w_2, w_3, w_4 , respectively. Regions where w is higher are more important is the L_5 -preprocessing-term (17) which controls the influence of the H α -fibrils.

306 (See Figure 4 bottom right panel.)

307 We now figure out the optimal value of μ_5 in Equation (11) for the four different
308 weighting functions $w_1 - w_4$. Initially, we use a step size of $\Delta\mu_5 = 0.05$ and then,
309 around the first appearing maximum, we reduced it to $\Delta\mu_5 = 0.005$. This is to
310 find a more precise optimal value of μ_5 . We calculate the Pearson correlation coeffi-
311 cient between the chromospheric reference field (\mathbf{B}_{ch}) and the minimum solution of
312 the preprocessing routine (\mathbf{B}_{pp}). This provides us the optimal values of μ_5 for the
313 different weighting functions, see second row in Table 1.

314 5. Results

315 Table 1 lists some metrics related to the various preprocessing schemes, including the
316 dimensionless numbers ϵ_{force} and ϵ_{torque} from Equations (9) and (10), the values
317 of the various L_n from Section 3, and the averaged angles between the prepro-
318 cessing results and the model-chromospheric field. The first three rows of the table
319 list the model chromosphere (B_{ch}) and photosphere (B_{ph}) data and the classical
320 preprocessing scheme (B_{cp}). When using the unprocessed model-photospheric data
321 (B_{ph}), it is clear that the force-free consistency criteria (as represented by L_{12} ,
322 ϵ_{force} , and ϵ_{torque}) are not fulfilled and are orders of magnitude higher than for the
323 chromospheric data (B_{ch}). Consequently, we cannot expect the extrapolation codes
324 to result in a meaningful nonlinear force-free field in the corona, as discussed in
325 Metcalf *et al.* (2007).

326 The remaining rows in Tables 1 and 2 list the results for the cases where the H α
327 preprocessing was used. A qualitative comparison of the H α -preprocessed magne-
328 tograms (shown in Figure 5) with the model chromosphere (shown in the top panel
329 of Figure 1) indicates a strong resemblance for all three magnetic field components,
330 but certainly not a perfect match. Difference images between the H α -preprocessed
331 magnetograms and the model chromosphere (shown in the top panel of Figure 1)
332 are present in Figure 6. The resemblance using the H α preprocessing scheme is
333 much improved when compared to the magnetograms resulting from the classical
334 preprocessing scheme.

335 Table 2 displays metrics of the resulting nonlinear force-free extrapolations using
336 each preprocessing scheme.² As expected, the extrapolation codes perform poorly
337 when the unprocessed boundary (B_{ph}) is used. In particular, the resulting magnetic
338 energy ϵ_{mag} of this case (normalized to the energy of the reference solution) is only
339 65% of the correct answer, making it almost impossible to estimate the free magnetic
340 energy in the solution available for release during eruptive processes such as flares
341 and coronal mass ejections.

342 Taking preprocessing into account (rows 3-7 in both tables) significantly improves
343 the result. The force-free consistency criteria (L_{12} , ϵ_{force} , ϵ_{torque}) are adequately
344 fulfilled for all preprocessed cases and are even better (lower values) than the model
345 chromospheric field. This is naturally, however, because the preprocessing routine has
346 been developed in particular to derive force-free-consistent boundary conditions from

²For an explanation of the extrapolation method used to perform the results in Table 2, see appendix A and references therein. An explanation of the vector comparison metrics used in the table is given in Appendix B.

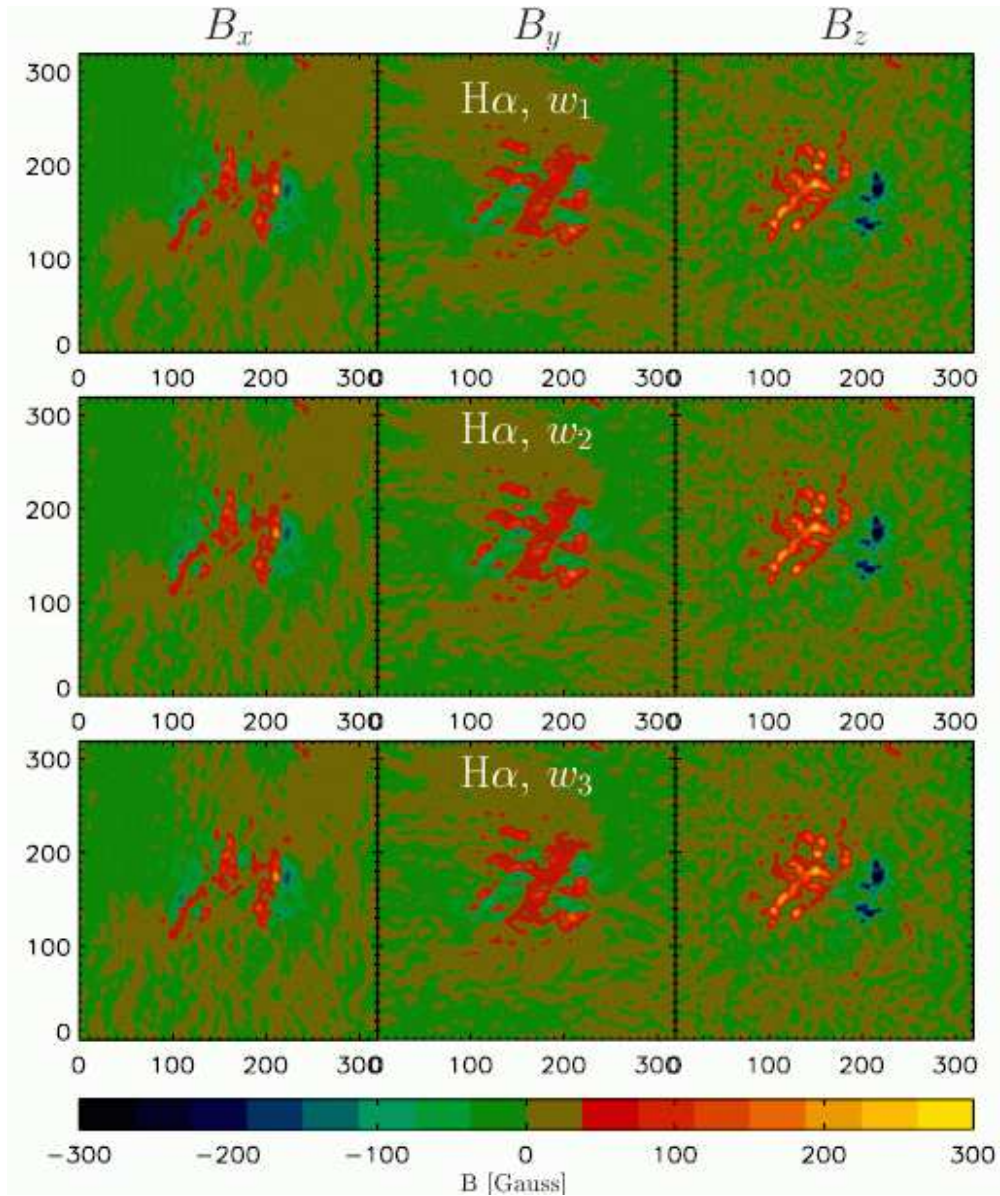


Figure 5. Results of $H\alpha$ preprocessing with different weighting functions. Top: w_1 , Center: w_2 , Bottom: w_3 , see text.

347 inconsistent (forced, noisy) photospheric measurements. The classical preprocessing
 348 (B_{cp}) has already reduced the angle to the model $H\alpha$ fibrils (last two columns of
 349 Table 1) by almost a factor of two, even though no information about the chromo-
 350 sphere has been used. If we include chromospheric information, (see Figure 4) in
 351 our preprocessing routine ($B_{H\alpha p}$, rows 4-7) the angle of the preprocessed field with
 352 the $H\alpha$ images reduces significantly. The second to last row in Table 1 contains the

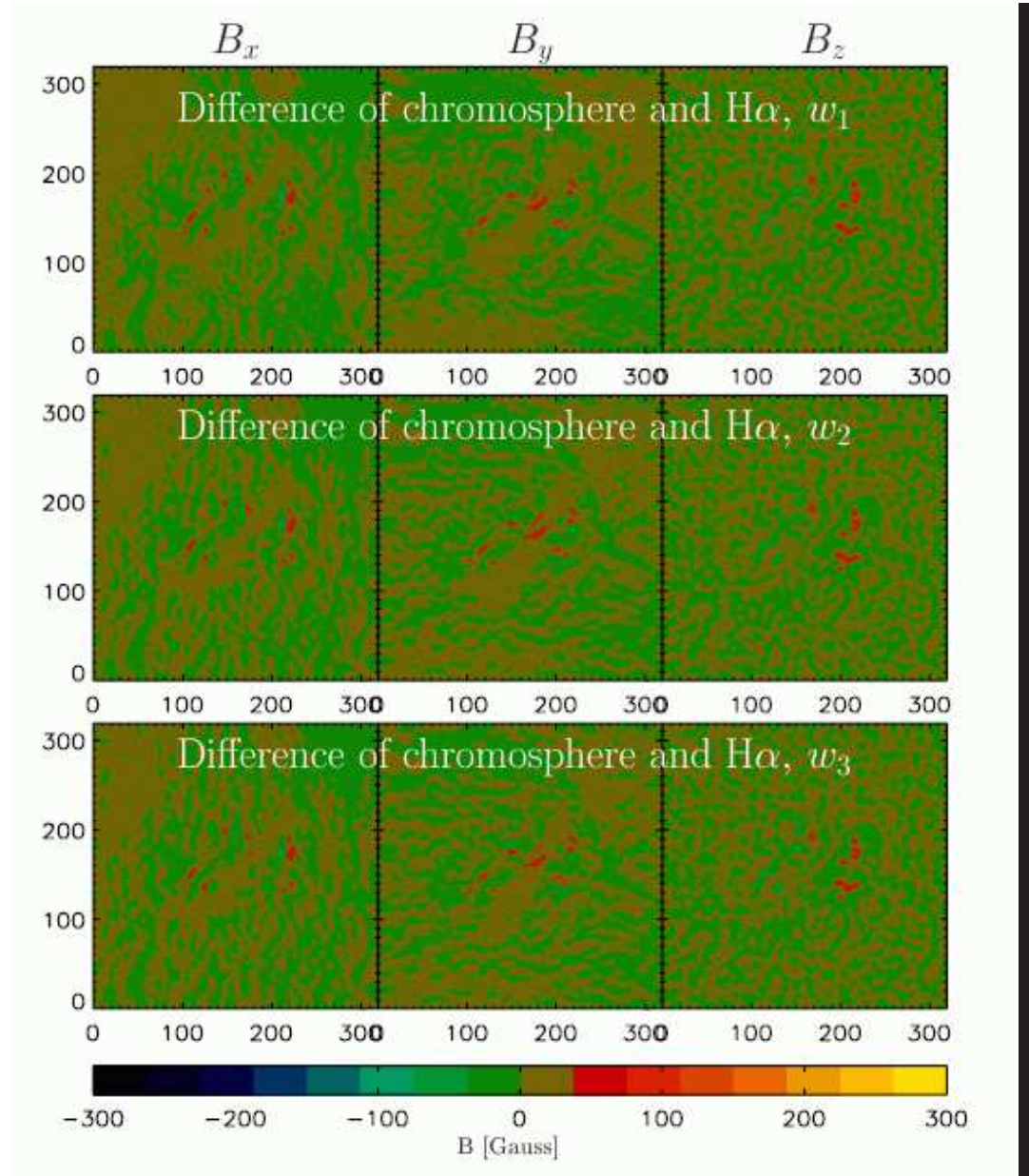


Figure 6. Differences of the chromospheric model field (see top panel of Figure 2 and the H α -preprocessed fields as shown in Figure 5).

average angle and in the last column the angle has been weighted by the magnetic field, which means that $\phi_{\text{ave},w}$ measures mainly how well the magnetic field and the chromospheric fibrils are aligned in regions of a high magnetic field strength. For the purpose of coronal magnetic field extrapolations the strong field regions are essential. If we include all information from the $H\alpha$ image, as done in row 4 for w_1 we find that the magnetic field and the fibrils are almost parallel in the entire region. This is the ideal case, however, as fibrils have been identified all over the region with the same excellent accuracy. For observed data it is more likely that the direction of the fibrils will be identifiable with high accuracy only in bright and magnetically strong regions. This effect is taken into account in rows 5-7 of both tables. In the last two rows we take the chromospheric data only into account where the magnetic field strength is larger than 50% and 10% of the maximum field strength, respectively. Naturally, the average angle ϕ_{ave} of the chromospheric fibrils with the preprocessed magnetic field becomes larger than for the ideal case. We find, however, that the angle $\phi_{\text{ave},w}$ remains relatively low in strong field regions, except for the case w_3 .

We can easily understand that w_3 (chromospheric information ignored where the magnetic field is less than 50% of its maximum) provides less accurate results, because the area where chromospheric data have been taken into account, is only a very small fraction of the entire region (see Figure 4 lower central panel).

Case w_3 has few nonzero points. These points are, however, in the regions with the strongest magnetic field strength. The L_5 terms minimizes the angle between magnetic field and chromospheric fibrils only in these nonzero points. This local correction does, however, influence the magnetogram globally, because the L_1 and L_2 term contain global measures and the L_4 terms couples neighbouring points. As a consequence the preprocessing result is different from classical preprocessing, even if the L_5 term is nonzero only for a limited number of pixel.

For observational data the weighting w_4 (last row in the tables, areas with less than 10% ignored; see also 4 lower right panel) seems to be more realistic. In this case the overall average angle is not better than for classical preprocessing, but is different by only about 3° when preferential weighting is given to the more important strong field regions.

The ultimate test regarding the success of our extended preprocessing scheme is to use the preprocessed field as boundary conditions for a nonlinear force-free coronal magnetic field extrapolation. The results are presented in Table 2, row 3 for classical preprocessing and rows 4-7 for $H\alpha$ preprocessing. We find that all preprocessed fields provide much better results than using the unprocessed data. For classical preprocessing we get the magnetic energy ϵ_{mag} correct with an error of 3% (for unprocessed data we got an error of 35%). Taking the $H\alpha$ information into account improves the result and the magnetic energy is computed with an accuracy of 1% or better, even for the cases where we used chromospheric information only in parts of the entire regions.

6. Conclusions and Outlook

Within this work we developed an improved algorithm for the preprocessing of photospheric vector magnetograms for the purpose of getting suitable boundary conditions for nonlinear force-free extrapolations. We extended the preprocessing routine developed by Wiegelmann, Inhester, and Sakurai (2006), which is referred to

Table 1. Results of the various preprocessing schemes: the model chromosphere and photosphere (first two rows), classical preprocessing (third row), and the H α preprocessing cases (last four rows). Column 1 identifies the data set, columns 2 and 3 the value of μ_5 and the weighting scheme used for the H α preprocessing cases. Columns 4-7 provide the value of the functionals $L_{12} = L_1 + L_2$, L_3 , L_4 , L_5 as defined in Equations (12)-(15) and (17), respectively. In columns 8 and 9 we show how well the force-free and torque-free consistency criteria ($\varepsilon_{\text{force}}$, $\varepsilon_{\text{torque}}$) as defined in Equations (9) and (10) are fulfilled. The last two columns contain the averaged angle ($\phi_{\text{ave}} = \langle \phi(x, y) \rangle$) of the field with the model chromospheric data and a magnetic field weighted average angle ($\phi_{\text{ave,w}} = \frac{\langle B^2 \phi(x, y) \rangle}{\langle B^2 \rangle}$) with $\phi(x, y)$ as defined in Equation (16).

Data	Weights		$L_{\text{prep}} \times 10^{-6}$				Aly criteria		ϕ_{ave}	$\phi_{\text{ave,w}}$
	μ_5	w	L_{12}	L_3	L_4	L_5	$\varepsilon_{\text{force}}$	$\varepsilon_{\text{torque}}$	[deg]	[deg]
B_{ch}	-	-	452.137	3.57	0.18	0.00	0.0171	0.0203	—	—
B_{np}	-	-	338287.	0.00	4.45	0.49	0.4138	0.5797	19.2	18.9
B_{cp}	-	-	0.06658	2.30	0.18	0.21	0.0003	0.0001	10.1	8.8
$B_{\text{H}\alpha\text{p}}$	1.525	w ₁	33.37	2.45	0.17	0.0007	0.0062	0.0011	1.1	0.4
$B_{\text{H}\alpha\text{p}}$	1.765	w ₂	31.70	2.47	0.15	0.0171	0.0060	0.0012	7.3	2.0
$B_{\text{H}\alpha\text{p}}$	1.880	w ₃	29.10	2.41	0.15	0.1355	0.0058	0.0012	10.8	6.8
$B_{\text{H}\alpha\text{p}}$	2.115	w ₄	32.16	2.41	0.17	0.0531	0.0060	0.0012	10.4	3.1

Table 2. Results of the nonlinear force-free field extrapolations in a 3D box ($320 \times 320 \times 256$). The rows are the same as in Table 1. The first three columns identify the preprocessing scheme, the value of μ_5 , and the weighting scheme as in Table 1. The fourth column contains the functional L , as defined in Equation (21), which tells us how well the force-free and solenoidal conditions are fulfilled in the computational box. In columns 5-9 we compare the extrapolated 3D magnetic field with the reference solution and use different quantitative comparison metrics: the vector correlation (C_{vec}), the Cauchy-Schwarz metric (C_{cs}), the complement of the normalized vector error (E'_{n}), the complement of the mean vector error (E'_{m}), and the total magnetic energy normalized to the reference field (ϵ_{mag}) as defined in Equations (22)-(26), respectively. Perfect agreement for any of these comparison metrics is unity.

Data	μ_5	w	L	C_{vec}	C_{cs}	E'_{n}	E'_{m}	ϵ_{mag}
B_{ch}	-	-	0.53	1.00	1.00	1.00	1.00	1.00
B_{np}	-	-	46.03	0.91	0.99	0.69	0.85	0.65
B_{cp}	-	-	5.99	0.97	0.99	0.80	0.85	0.97
$B_{\text{H}\alpha\text{p}}$	1.525	w ₁	3.45	0.97	1.00	0.81	0.85	1.01
$B_{\text{H}\alpha\text{p}}$	1.765	w ₂	2.37	0.97	1.00	0.81	0.86	1.00
$B_{\text{H}\alpha\text{p}}$	1.880	w ₃	2.31	0.97	1.00	0.81	0.85	0.99
$B_{\text{H}\alpha\text{p}}$	2.115	w ₄	3.20	0.97	1.00	0.81	0.85	1.00

here as “classical preprocessing”. The main motivation for this work is related to the fact that active-region coronal magnetic fields are force-free due to the low β coronal plasma, but the magnetic field vector can be measured with high accuracy only on the photosphere, where the plasma β is about unity and non-magnetic forces cannot be ignored. Our original (“classical”) preprocessing removes these non-magnetic forces and makes the field compatible with the force-free assumption leading to more chromospheric-like configurations. In this study, we have found that by taking direct chromospheric observations into account (such as by using fibrils seen in $H\alpha$ images), the preprocessing is improved beyond the classical scheme. This improved scheme includes a term which minimizes the angle between the preprocessed magnetic field and the fibrils. We tested our method with the help of a model active region developed by van Ballegoijen *et al.* (2007), which includes the forced photospheric and force-free chromospheric and coronal layers. This model has been used by Metcalf *et al.* (2007) for an inter-comparison of nonlinear force-free extrapolation codes. The comparison revealed that the model coronal magnetic field was reconstructed very well if chromospheric magnetic fields have been used as input, but in contrast the reconstructed fields compared poorly when unprocessed model-photospheric data were used. Classical preprocessing significantly improves the result, but the $H\alpha$ preprocessing developed in this paper is even better as the main features of the model corona are reconstructed with high accuracy. Our extended preprocessing tool provides a fair estimate of the chromospheric magnetic field, which is used as boundary condition for computing the nonlinear force-free coronal magnetic field. In particular, the magnetic energy in the force-free domain above the chromosphere agrees with the model corona within 1%, even if only strong-field regions of the model chromosphere, where the fibrils can be identified with highest accuracy, influence the final solution. From these tests we conclude that our improved preprocessing routine is a useful tool for providing suitable boundary conditions for the computation of coronal magnetic fields from measured photospheric vector magnetograms as provided for example from *Hinode*. The combination of preprocessing and nonlinear force-free field extrapolations seem likely to provide accurate computation of the magnetic field in the corona.

We will still not get the magnetic field structure in the relative thin layer between/in the photosphere and the chromosphere correct, because here non-magnetic forces cannot be neglected due to the finite β plasma. Although this layer is vertically thin (*e.g.*, 2 vertical grid points in the van Ballegoijen *et al.* (2007) model compared to 256 vertical grid points in the corona) it contains a significant part of the total magnetic energy of the entire domain, see Metcalf *et al.* (2007). Unfortunately, this part of the energy cannot be recovered by force-free extrapolations, because the region is non-force-free. Our improved preprocessing routine includes chromospheric information and therefore provides us with a closer approximation of the chromospheric magnetic field. This leads to more accurate estimates of the total magnetic energy in the corona.

A further improvement of the preprocessing routine could be done with the help of additional observations, *e.g.* the line-of-sight chromospheric field, as planned for SOLIS. One could include these measurement directly in the L_3 -term (14) either as the only information or in some weighted combination with the photospheric field measurement. An investigation of the true 3D-structure of the thin non-force-free layer between photosphere and chromosphere requires further research. First steps towards non-force-free magnetohydrostatic extrapolation codes (Wiegelmann and

Neukirch, 2006) might help to reveal the secrets of this layer. Non force-free magnetic field extrapolations will require additional observational constraints, because the magnetic field, the plasma density and pressure must be computed self-consistently in one model.

Acknowledgements The work of T. Wiegmann was supported by DLR-grant 50 OC 0501 and J.K. Thalmann got financial support by DFG-grant WI 3211/1-1. M. DeRosa, T. Metcalf, and C. Schrijver were supported by Lockheed Martin Independent Research funds. We acknowledge stimulating discussions during the fourth NLFFF-consortium meeting in June, 2007 in Paris.

Appendix

A. Extrapolation of Nonlinear Force-free Coronal Magnetic Fields

We briefly summarize our nonlinear force-free extrapolation code here, which has been used to compute the 3D magnetic fields. We solve the force-free Equations (1) and (2) by optimizing (minimizing) the following functional:

$$L = \int_V \left[w_a B^{-2} |(\nabla \times \mathbf{B}) \times \mathbf{B}|^2 + w_b |\nabla \cdot \mathbf{B}|^2 \right] d^3x, \quad (21)$$

where $w_a(x, y, z)$ and $w_b(x, y, z)$ are weighting functions. It is obvious that (for $w_a, w_b > 0$) the force-free equations (1) and (2) are fulfilled when L is zero. The optimization method was proposed by Wheatland, Sturrock, and Roumeliotis (2000) and further developed in Wiegmann and Neukirch (2003). Here we use the implementation of Wiegmann (2004) which has been applied to data in Wiegmann et al. (2005). In this article, we used a recent update including of our code that included a multi-scale approach (see Metcalf et al. (2007) for details). This version of the optimization code was also used with the (same as in this paper) model-chromospheric, photospheric and classical preprocessed photospheric magnetic field vector as part of an inter-code-comparison in (Metcalf et al., 2007). For alternative methods to solve the force-free Equations (1) and (2) see the review papers by (Sakurai, 1989; Aly, 1989; Amari et al., 1997; McClymont, Jiao, and Mikic, 1997; Wiegmann, 2008) and references therein.

B. Metrics to Compare a 3D Coronal Magnetic Field with a Reference Solution.

In order to quantify the degree of agreement between the extrapolated vector fields of the input model field (\mathbf{B} , *i.e.*, the extrapolated chromospheric (reference) field) and the nonlinear force-free solutions (\mathbf{b} , *i.e.*, the extrapolated preprocessed photospheric field) that are specified on identical sets of grid points, we use five metrics in table 2 that compare either local characteristics or the global energy content in addition to the force and divergence integrals. These measures have been developed in Schrijver et al. (2006) and subsequently been used to evaluate the quality of force-free and non-force-free extrapolation codes (Amari, Boulmezaoud, and Aly, 2006; Wiegmann

485 *et al.*, 2006; Wiegelmann and Neukirch, 2006; Song *et al.*, 2006; Wiegelmann, 2007;
486 Metcalf *et al.*, 2007).

487 The vector correlation metric has been defined as

$$C_{\text{vec}} = \frac{\sum_i \mathbf{B}_i \mathbf{b}_i}{\sqrt{\sum_i |\mathbf{B}_i|^2 \sum_i |\mathbf{b}_i|^2}}, \quad (22)$$

488 where \mathbf{B}_i and \mathbf{b}_i are the vectors at each point i . One finds that $C_{\text{vec}} = 1$ if the
489 vector fields are identical and $C_{\text{vec}} = 0$ if $\mathbf{B}_i \perp \mathbf{b}_i$.

490 The Cauchy-Schwarz metric is based on the homonymous inequality ($|\mathbf{a} \cdot \mathbf{c}| \leq |\mathbf{a}| |\mathbf{c}|$)
491 for any two vectors \mathbf{a} and \mathbf{c})

$$C_{\text{cs}} = \frac{1}{M} \sum_i \frac{\mathbf{B}_i \cdot \mathbf{b}_i}{|\mathbf{B}_i| |\mathbf{b}_i|} \equiv \frac{1}{M} \sum_i \cos \theta_i, \quad (23)$$

492 where M is the total number of vectors in the volume, and θ_i the angle between \mathbf{B}
493 and \mathbf{b} at point i . It is entirely a measure of the angular differences of the vector
494 fields, i. e. $C_{\text{cs}} = 1$ if $\mathbf{B} \parallel \mathbf{b}$, $C_{\text{vec}} = -1$ if they are anti-parallel, and $C_{\text{vec}} = 0$ if
495 $\mathbf{B}_i \perp \mathbf{b}_i$ at each point.

496 The normalized vector error is defined as

$$E_{\text{n}} = \frac{\sum_i |\mathbf{b}_i - \mathbf{B}_i|}{\sum_i |\mathbf{B}_i|}. \quad (24)$$

497 The mean vector error averages over relative differences and is given by

$$E_{\text{m}} = \frac{1}{M} \sum_i \frac{|\mathbf{b}_i - \mathbf{B}_i|}{|\mathbf{B}_i|}. \quad (25)$$

498 Unlike the first two metrics, perfect agreement of the two vector fields results in
499 $E_{\text{m}} = E_{\text{n}} = 0$. For an easier comparison with the others, we list $E'_{\text{m,n}} \equiv 1 - E_{\text{m,n}}$,
500 so that all measures reach unity for a perfect match.

501 To estimate how well the models rates the energy content of the field, we use the
502 total magnetic energy of \mathbf{b} , normalized to the total magnetic energy of \mathbf{B} , namely

$$\epsilon_{\text{mag}} = \frac{\sum_i |\mathbf{b}_i|^2}{\sum_i |\mathbf{B}_i|^2}. \quad (26)$$

503 References

- 504 Aly, J.J.: 1989, On the reconstruction of the nonlinear force-free coronal magnetic field from
505 boundary data. *Sol. Phys.* **120**, 19–48.
506 Amari, T., Aly, J.J., Luciani, J.F., Boulmezaoud, T.Z., Mikic, Z.: 1997, Reconstructing the
507 Solar Coronal Magnetic Field as a Force-Free Magnetic Field. *Sol. Phys.* **174**, 129–149.
508 Amari, T., Boulmezaoud, T.Z., Aly, J.J.: 2006, Well posed reconstruction of the solar coronal
509 magnetic field. *A&A* **446**, 691–705. doi:10.1051/0004-6361:20054076.
510 Gary, G.A.: 2001, Plasma Beta above a Solar Active Region: Rethinking the Paradigm. *Sol.*
511 *Phys.* **203**, 71–86.

- Inhester, B., Feng, L., Wiegmann, T.: 2007, Segmentation of loops from coronal EUV images. *Sol. Phys.* **in press**.
- Kramar, M., Inhester, B., Solanki, S.K.: 2006, Vector tomography for the coronal magnetic field. I. Longitudinal Zeeman effect measurements. *A&A* **456**, 665–673. doi:10.1051/0004-6361:20064865.
- Lin, H., Kuhn, J.R., Coulter, R.: 2004, Coronal Magnetic Field Measurements. *ApJL* **613**, L177–L180. doi:10.1086/425217.
- Low, B.C., Lou, Y.Q.: 1990, Modeling solar force-free magnetic fields. *ApJ* **352**, 343–352.
- McClymont, A.N., Jiao, L., Mikic, Z.: 1997, Problems and Progress in Computing Three-Dimensional Coronal Active Region Magnetic Fields from Boundary Data. *Sol. Phys.* **174**, 191–218.
- Metcalf, T.R., DeRosa, M.L., Schrijver, C.J., Barnes, G., VanBallegooijen, A., Wiegmann, T., Wheatland, M.S., Valori, G., McTiernan, J.M.: 2007, Non-linear force-free modeling of coronal magnetic fields. II. Modeling a filament arcade from simulated chromospheric and photospheric vector fields. *Sol. Phys.* **accepted**.
- Metcalf, T.R., Jiao, L., McClymont, A.N., Canfield, R.C., Uitenbroek, H.: 1995, Is the solar chromospheric magnetic field force-free? *ApJ* **439**, 474–481. doi:10.1086/175188.
- Molodensky, M.M.: 1969, Integral properties of force-free fields. *Soviet Astron.-AJ* **12**, 585–588.
- Molodensky, M.M.: 1974, Equilibrium and stability of force-free magnetic field. *Sol. Phys.* **39**, 393–404.
- Sakurai, T.: 1981, Calculation of Force-Free Magnetic Field with Non Constant Alpha. *Sol. Phys.* **69**, 343–+.
- Sakurai, T.: 1989, Computational modeling of magnetic fields in solar active regions. *Space Science Reviews* **51**, 11–48.
- Schrijver, C.J., Derosa, M.L., Metcalf, T.R., Liu, Y., McTiernan, J., Régnier, S., Valori, G., Wheatland, M.S., Wiegmann, T.: 2006, Nonlinear Force-Free Modeling of Coronal Magnetic Fields Part I: A Quantitative Comparison of Methods. *Sol. Phys.* **235**, 161–190. doi:10.1007/s11207-006-0068-7.
- Schrijver, C.J., van Ballegooijen, A.A.: 2005, Is the Quiet-Sun Corona a Quasi-steady, Force-free Environment? *ApJ* **630**, 552–560. doi:10.1086/431754.
- Solanki, S.K., Lagg, A., Woch, J., Krupp, N., Collados, M.: 2003, Three-dimensional magnetic field topology in a region of solar coronal heating. *Nature* **425**, 692–695.
- Song, M.T., Fang, C., Tang, Y.H., Wu, S.T., Zhang, Y.A.: 2006, A New and Fast Way to Reconstruct a Nonlinear Force-free Field in the Solar Corona. *Astrophys. J.* **649**, 1084–1092. doi:10.1086/506249.
- van Ballegooijen, A.A.: 2004, Observations and Modeling of a Filament on the Sun. *ApJ* **612**, 519–529. doi:10.1086/422512.
- van Ballegooijen, A.A., Deluca, E.E., Squires, K., Mackay, D.H.: 2007, Modeling magnetic flux ropes in the solar atmosphere. *Journal of Atmospheric and Terrestrial Physics* **69**, 24–31. doi:10.1016/j.jastp.2006.06.007.
- Wheatland, M.S., Sturrock, P.A., Roumeliotis, G.: 2000, An Optimization Approach to Reconstructing Force-free Fields. *ApJ* **540**, 1150–1155.
- Wiegmann, T.: 2004, Optimization code with weighting function for the reconstruction of coronal magnetic fields. *Sol. Phys.* **219**, 87–108.
- Wiegmann, T.: 2007, Computing Nonlinear Force-Free Coronal Magnetic Fields in Spherical Geometry. *Sol. Phys.* **240**, 227–239. doi:10.1007/s11207-006-0266-3.
- Wiegmann, T.: 2008, Nonlinear force-free modeling of the solar coronal magnetic field.. *J. Geophys. Res.* **VOL. 113**, A03S02, doi:10.1029/2007JA012432.
- Wiegmann, T., Inhester, B., Kliem, B., Valori, G., Neukirch, T.: 2006, Testing non-linear force-free coronal magnetic field extrapolations with the Titov-Démoulin equilibrium. *A&A* **453**, 737–741. doi:10.1051/0004-6361:20054751.
- Wiegmann, T., Inhester, B., Lagg, A., Solanki, S.K.: 2005, How To Use Magnetic Field Information For Coronal Loop Identification. *Sol. Phys.* **228**, 67–78. doi:10.1007/s11207-005-2511-6.
- Wiegmann, T., Inhester, B., Sakurai, T.: 2006, Preprocessing of vector magnetograph data for a nonlinear force-free magnetic field reconstruction. *Sol. Phys.* **233**, 215–232.
- Wiegmann, T., Neukirch, T.: 2003, Computing nonlinear force free coronal magnetic fields. *Nonlinear Processes in Geophysics* **10**, 313–322.
- Wiegmann, T., Neukirch, T.: 2006, An optimization principle for the computation of MHD equilibria in the solar corona. *A&A* **457**, 1053–1058. doi:10.1051/0004-6361:20065281.

